Room temperature continuous wave operation and controlled spontaneous emission in ultrasmall photonic crystal nanolaser

Kengo Nozaki, Shota Kita and Toshihiko Baba

Yokohama National University, Department of Electrical and Computer Engineering
79-5 Tokiwadai, Hodogayaku, Yokohama 240-8501, Japan
Email: baba@ynu.ac.jp

Abstract: Photonic crystal slab enables us to form an ultrasmall laser cavity with a modal volume close to the diffraction limit of light. However, the thermal resistance of such nanolasers, as high as 10^6 K/W, has prevented continuous-wave operation at room temperature. The present paper reports on the first successful continuous-wave operation at room temperature for the smallest nanolaser reported to date, achieved through fabrication of a laser with a low threshold of 1.2 μW. Near-thresholdless lasing and spontaneous emission enhancement due to the Purcell effect are also demonstrated in a moderately low *Q* nanolaser, both of which are well explained by a detailed rate equation analysis.

OCIS codes: (140.5960) Semiconductor lasers; (230.3990) Microstructure devices

References and links

1. T. H. Maiman, "Stimulated optical radiation in ruby," Nature **187**, 493–494 (1960).
2. I. Hayashi, M. B. Panish, P. W. Foy and S. Sumski, "Junction lasers which operate continuously at room temperature," Appl. Phys. Lett. **17**, 109–111 (1970).
3. K. Iga, F. Koyama and S. Kinoshita, "Surface emitting semiconductor lasers," IEEE J. Quantum Electron., **24**, 1845–1855 (1988).
4. J. L. Jewell, J. P. Harbison, A. Scherer, Y. H. Lee and L. T. Florez, "Vertical-cavity surface emitting lasers: design, growth, fabrication, characterization," IEEE J. Quantum Electron. **27**, 1332–1347 (1991).
5. S. L. McCall, A. F. J. Levi, R. E. Slusher, S. J. Pearton and R. A. Logan, "Whispering gallery mode microdisk lasers," Appl. Phys. Lett. **60**, 289–291 (1992).
6. O. Painter, R. K. Lee, A. Scherer, A. Yariv, J. D. O'Brien, D. D. Dapkus, and I. Kim, "Two dimensional photonic band-gap defect mode laser," Science **284**, 1819–1821 (1999).
7. E. M. Purcell, "Spontaneous emission probabilities at radio frequencies," Phys. Rev. **69**, 681 (1946).
8. T. Kobayashi, Y. Morimoto and T. Sueta, "Closed microcavity laser," Nat. Top. Meet. Rad. Sci. RS85-06 (1985).
9. E. Yablonovitch and T. J. Gmitter, "Inhibited spontaneous emission in solid state physics and electronics," Phys. Rev. Lett. **58**, 2059–2062 (1987).
10. Y. Yamamoto, ed., "*Coherence, Amplification, and Quantum effects in Semiconductor Lasers*," (John Wiley & Sons, New York, 1991).
11. H. Yokoyama and K. Ujihara, eds., "*Spontaneous Emission and Laser Oscillation in Microcavities*," (CRC Press, New York, 1995).
12. T. Baba, "Photonic crystals and microdisk cavities based on GaInAsP-InP system," IEEE J. Sel. Top. Quantum Electron. **3**, 808–830 (1997).
13. J. M. Gérard and B. Gayral, "Strong purcell effect for InAs quantum boxes in three-dimensional solid-state microcavities," J. Lightwave Technol. **17**, 2089–2095 (1999).
14. M. Loncâr, T. Yoshie, A. Scherer, P. Gogna and Y. Qiu, "Low-threshold photonic crystal laser," Appl. Phys. Lett. **81**, 2680–2682 (2002).
15. H. Y. Ryu, M. Notomi, E. Kuramochi, and T. Segawa, "Large spontaneous emission factor (>0.1) in the photonic crystal monopole-mode laser," Appl. Phys. Lett. **84**, 1067–1069 (2004).
16. T. Baba, D. Sano, K. Nozaki, K. Inoshita, Y. Kuroki and F. Koyama, "Observation of fast spontaneous emission decay in GaInAsP photonic crystal point defect nanocavity at room temperature," Appl. Phys. Lett. **85**, 3989–3991 (2004).
17. T. Baba and D. Sano, "Low threshold lasing and Purcell effect in microdisk lasers at room temperature," IEEE J. Sel. Top. Quantum Electron. **9**, 1340–1346 (2003).

#82246 - $15.00 USD Received 19 Apr 2007; revised 28 May 2007; accepted 28 May 2007; published 4 Jun 2007

18. R. Coccioli, M. Boroditsky, K.W. Kim, Y. Rahmat-Samii and E. Yablonovitch, “Smallest possible electromagnetic mode volume in a dielectric cavity,” IEE Proc.-Optoelectron. **145**, 391–397 (1998).
19. Z. Zhang and M. Qiu, “Small-volume waveguide-section high *Q* microcavities in 2D photonic crystal slabs,” Opt. Exp. **12**, 3988–3995 (2004).
20. K. Nozaki, T. Ide, J. Hashimoto, W. H. Zheng and T. Baba, “Photonic crystal point shift nanolaser with ultimate small modal volume,” Electron. Lett. **41**, 843–845 (2005).
21. K. Nozaki and T. Baba, “Laser characteristics with ultimate-small modal volume in photonic crystal slab point-shift nanolasers,” Appl. Phys. Lett. **88**, 211101 (2006).
22. K. Inoshita and T. Baba, “Fabrication of GaInAsP/InP photonic crystal lasers by ICP etching and control of resonant mode in point and line composite defects,” IEEE J. Sel. Top. Quantum Electron. **9**, 1347–1354 (2003).
23. J. K. Hwang, H. Y. Ryu, D. S. Song, I. Y. Han, H. K. Park, D. H. Jang and Y. H. Lee, “Continuous room-temperature operation of optically pumped two-dimensional photonic crystal lasers at 1.6 μm,” Photon. Tech. Lett. **12**, 1295–1297 (2000).
24. M. Nomura, S. Iwamoto, K. Watanabe, N. Kumagai, Y. Nakata, S. Ishida, and Y. Arakawa, “Room temperature continuous-wave lasing in photonic crystal nanocavity,” Opt. Exp. **14**, 6308–6315 (2006).
25. D. Englund, D. Fattal, E. Waks, G. Solomon, B. Zhang, T. Nakaoka, Y. Arakawa, Y. Yamamoto and J. Vučković, “Controlling the spontaneous emission rate of single quantum dots in a two-dimensional photonic crystal,” Phys. Rev. Lett. **95**, 013904 (2005).
26. W. H. Chang, W. Y. Chen, H. S. Chang, T. P. Hsieh, J. I. Chyi and T. M. Hsu, “Efficient single-photon sources based on low-density quantum dots in photonic-crystal nanocavities,” Phys. Rev. Lett. **96**, 117401 (2006).
27. M. Fujita, A. Sugitatsu, T. Uesugi and S. Noda, “Fabrication of indium phosphide compound photonic crystal by iodine/xenon inductively coupled plasma etching,” Jpn. J. Appl. Phys. **43**, L1400–1402 (2004).
28. T. Ide, J. Hashimoto, K. Nozaki, E. Mizuta and T. Baba, “InP etching by HI/Xe inductively coupled plasma for photonic-crystal device fabrication,” Jpn. J. Appl. Phys. **45**, L102–L104 (2006).
29. K. Nozaki, A. Nakagawa, D. Sano and T. Baba, “Ultralow threshold and singlemode lasing in microgear lasers and its fusion with quasiperiodic photonic crystals,” IEEE J. Sel. Top. Quantum Electron. **9**, 1355–1360 (2003).
30. K. Nozaki and T. Baba, “Carrier and photon analyses of photonic microlasers by two-dimensional rate equations,” IEEE J. Sel. Area. Commun. **23**, 1411–1417 (2005).
31. M. Fujita, A. Sakai and T. Baba, “Ultra-small and ultra-low threshold microdisk injection laser – design, fabrication, lasing characteristics and spontaneous emission factor,” IEEE J. Sel. Top. Quantum Electron. **5**, 673–681 (1999).
32. J. Vučkovič, O. Painter, Y. Xu, A. Yariv and A. Scherer, “Finite-difference time-domain calculation of the spontaneous emission coupling factor in optical microcavities,” IEEE J. Quantum Electron. **35**, 1168–1175 (1999).
33. Y. Suematsu and S. Akiba, “High-speed pulse modulation of injection lasers at non-bias condition,” Trans. IECE of Japan **59**, 1–8 (1976).
34. H. Ichikawa, K. Inoshita and T. Baba, “Reduction in surface recombination of GaInAsP/InP micro-columns by CH_4 plasma irradiation,” Appl. Phys. Lett., **78**, 2119–2121 (2001).

1. Introduction

Lasers have been greatly miniaturized over the past few decades, from meter scale to micrometer scale [1–6], providing a range of improvements including reduction in lasing threshold, photonic integration, and cavity quantum electrodynamic effects such as spontaneous emission control and thresholdless operation [7–13]. Using a photonic crystal (PC), it is now possible to construct a nanometer-scale laser with a modal volume close to the diffraction limit of light [6, 14–16]. In such a nanolaser, the coupling of spontaneous emission (SpE) to a laser mode and the rate of SpE are enhanced by the Purcell effect [7]. For electric dipoles located at an antinodal position of the laser mode, the Purcell factor (F) can be approximated as $F = a_p\lambda^4/(2\pi^2 n^3 \Delta\lambda V_m)$ [17], where a_p is the normalized average projection component of electric dipoles on the electric field of the laser mode, λ is the modal wavelength, n is the material index, V_m is the modal volume defined by $V_m = \iiint n^2E^2 dxdydz/[n^2E^2]_{max}$ [6, 18] (This V_m is not equal to the physical volume of the mode, but includes the interaction effect between the laser mode and a single dipole located at antinodal position of the mode. The physical volume is given by $8V_m$.), and $\Delta\lambda$ is the wider spectral linewidth between the homogeneous broadening and the cavity resonance. As $\Delta\lambda$ is often thought to be dominated by cavity Q, high-Q cavities have been the target of extensive

#82246 - $15.00 USD Received 19 Apr 2007; revised 28 May 2007; accepted 28 May 2007; published 4 Jun 2007

study. However, high Q is no longer effective when the homogeneous broadening is wider than the cavity resonance. F is also enhanced in a simple manner by reducing V_m, which is a particular feature of photonic crystals (PCs). The present authors recently fabricated a point-shift PC nanolaser consisting solely of the shift of two lattice points in a PC slab with GaInAsP quantum well (The first idea of the cavity was reported by Zhang et al. [19] We call it the H0 nanolaser in this paper), and were successful in demonstrating pulsed laser operation at room temperature (RT) [20, 21]. Fitting of theoretical results to experimental values indicates that the laser mode consists of one primary antinode at the cavity center, with $V_m = 0.019\ \mu m^3$ (ca. $0.15(\lambda/n)^3$), close to the lower limit for an optical cavity [19, 21]. However, continuous wave (CW) operation at RT was not achieved due to the high thermal resistance of the device ($>10^6$ K/W) [22] and short nonradiative recombination lifetime (ca. 1 ns). It has thus been difficult to evaluate the SpE behavior below the lasing threshold reliably. RT CW operation has to date only been achieved using larger cavities (1–10 μm) [23, 24], with SpE control generally tested at cryogenic temperatures [25, 26]. In the present study, three key advancements are realized. The first achievement is RT CW operation of the H0 nanolaser, obtained through refinement of the GaInAsP/InP etching process leading to a dramatic reduction in the effective lasing threshold to a few-μW regime. Near-thresholdless operation and SpE enhancement through the Purcell effect are also demonstrated in CW condition and time-domain measurements. The theoretical results obtained by detailed rate equation analysis are confirmed to be consistent with the experimental observations, accounting for various effects such as nonradiative recombination, carrier diffusion, and photon recycling. An important conclusion suggested in this analysis is that a moderately low cavity Q as well as the strong Purcell effect is required for the thresholdless operation.

2. Evaluation of room temperature CW lasing characteristics

2.1. Device fabrication

A single point defect nanolaser (H1 nanolaser) was also fabricated for comparison with the H0 nanolaser. For the construction of both lasers, GaInAsP/InP quantum well (QW) wafers with a photoluminescence peak at $\lambda = 1.55\ \mu m$ were used as substrates. The PC slab was formed by electron beam lithography, HI/Xe inductively coupled plasma etching of the active layer [27, 28], and finally HCl wet etching of the InP cladding layers. The use of HI gas makes it possible to conduct direct etching using the electron beam resist mask near RT (ca. 70 °C), substantially simplifying the overall process and improving the smoothness of the etching profiles compared to conventional Cl_2-based processes. Figure 1 shows scanning electron micrographs of the H0 nanolaser thus fabricated. The sidewall roughness of holes is less than 10 nm. Figures 2(a) and 2(b) show the top view of the H0 nanolaser and the modal distribution (magnetic field normal to the slab, H_z) calculated by the finite-difference time-domain (FDTD) method, respectively, which affords an accurate model of the fabricated device with slab thickness and index of 140 nm and 3.4, respectively. Theoretically, the monopole mode has an ultrasmall V_m of $0.019\ \mu m^3 = 0.15(\lambda/n)^3$ and a high passive Q of 1.3×10^5. Figures 3(a) and 3(b) show the corresponding results for the H1 nanolaser. In this case, the innermost holes are 85% of the diameter of outer holes. This device supports orthogonal dipole modes with a larger V_m of $0.028\ \mu m^3 = 0.28(\lambda/n)^3$ and a lower Q of 1.1×10^3.

#82246 - $15.00 USD Received 19 Apr 2007; revised 28 May 2007; accepted 28 May 2007; published 4 Jun 2007

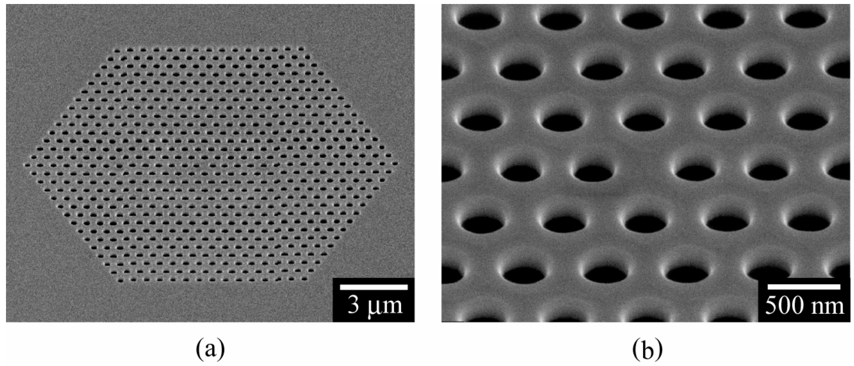

Fig. 1. Scanning electron micrograph of fabricated device. (a) Whole device. (b) Magnified view of the H0 nanolaser. Center two airholes are laterally shifted.

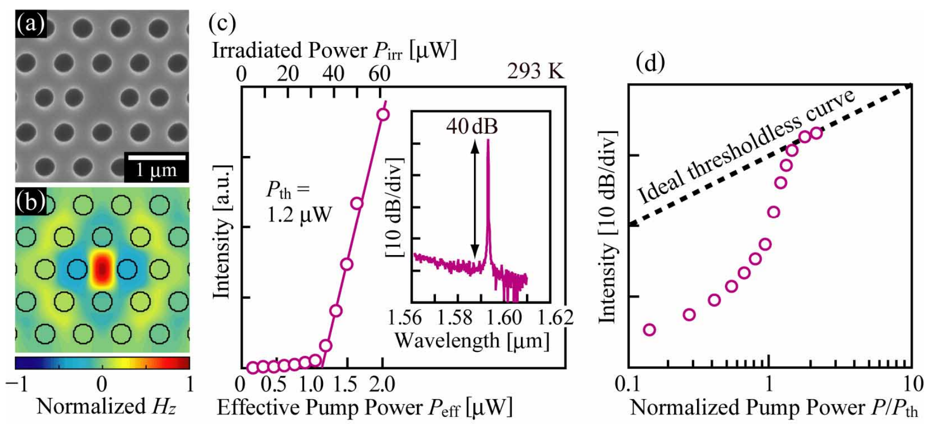

Fig. 2. CW lasing characteristic of H0 nanolaser with lattice constant a = 560 nm, normalized hole diameter $2r/a = 0.57$, and normalized hole shift $s/a = 0.28$. (a) Scanning electron micrograph of fabricated device (top view). (b) Calculated modal distribution (H_z). (c) Mode intensity characteristic and lasing spectrum above the lasing threshold. (d) Logarithmic plots of modal intensity versus normalized pump power characteristic.

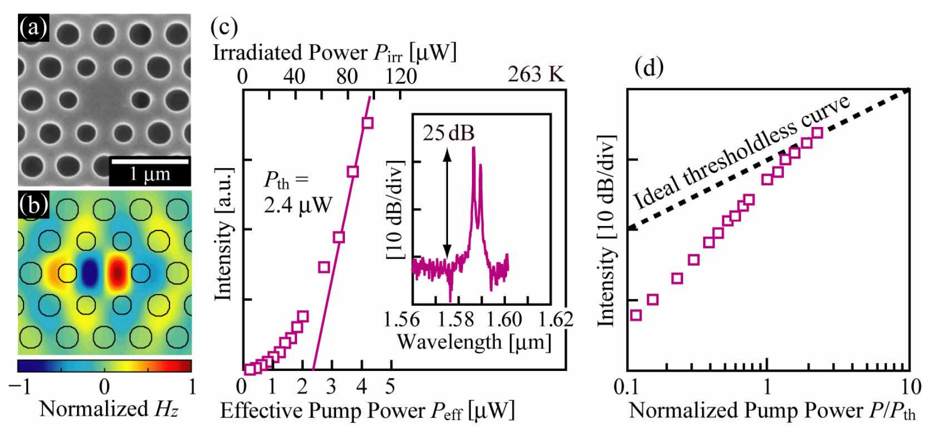

Fig. 3. CW lasing characteristic of H1 nanolaser with a = 480 nm, $2r/a = 0.62$, and normalized innermost hole diameter $2r'/a = 0.52$. (a) Scanning electron micrograph of fabricated device (top view). (b) Calculated modal distribution (H_z). (c) Mode intensity characteristics and lasing spectrum above the lasing threshold. (d) Logarithmic plots of modal intensity versus normalized pump power characteristic.

#82246 - $15.00 USD Received 19 Apr 2007; revised 28 May 2007; accepted 28 May 2007; published 4 Jun 2007

2.1. Measurement of lasing characteristics

Measurements involved photopumping the devices initially using a 0.98 μm CW laser with a spot diameter of 2.5 μm. Obvious lasing was observed only when the light spot coincided with the nanocavity. Figures 2(c) and 3(c) show the respective laser characteristics. The effective pump power (P_{eff}) was evaluated from the absorption efficiency of irradiated light in the slab (22%) [29] and the overlap efficiency with the nanocavity (15% for H0 and 20% for H1, in which the cavity area was assumed to be the ellipse attaching the innermost airholes). The H0 nanolaser exhibits a clear kink at a threshold of P_{eff} = 1.2 μW at RT (293 K), above which the single-mode spectrum of the monopole mode reaches a 40 dB peak over background and a resolution limit spectral width ($\Delta\lambda$) of 0.06 nm. At 0.8 times the threshold (the estimated transparent condition), $\Delta\lambda$ is 0.08 nm and the corresponding Q is 20,000. This is a reasonable value considering the theoretical passive Q and the free carrier absorption in the active region, although the H0 nanocavity theoretically has a higher Q of over 10^5. On the other hand, the H1 nanolaser exhibits dull kink at around P_{eff} = 2.4 μW. The double peak spectrum of dipole modes reaches a 25 dB peak near RT (263 K). In the transparent state, $\Delta\lambda$ is estimated to be 1.0 nm and the corresponding Q is 1,500, in close agreement with the theoretical value. As shown in Figs. 2(d) and 3(d), the logarithmic plots of the modal intensity characteristics clearly show that the H1 nanolaser exhibits near-thresholdless behavior, even though the weaker Purcell effect than that in H0 nanolaser would be expected from the larger modal volume.

3. Time-resolved measurement of emission decay

From the above equation, the Purcell factors (F) are calculated to be 25 and 13 for the H0 and H1 nanolasers, respectively, assuming typical parameters for the GaInAsP QW wafers at RT (a_p = 0.4, n = 3.4, and $\Delta\lambda$ = 8.8 nm for a homogeneous broadening of 4.3 meV) [17]. To evaluate the factor experimentally, the time-resolved measurement of the SpE intensity and decay at RT were carried out under pulsed photopumping at a wavelength of 0.975 μm using a pulse width of 90 ps and spot diameter of 3 μm. The SpE from the device was photon-counted using a photomultiplier tube (R3809-69, Hamamatsu), and the decay lifetime (τ) was determined by taking the deconvolution with respect to the pump pulse. The temporal resolution of the measurement was 100 ps, and the shortest limit of τ thus determined was of

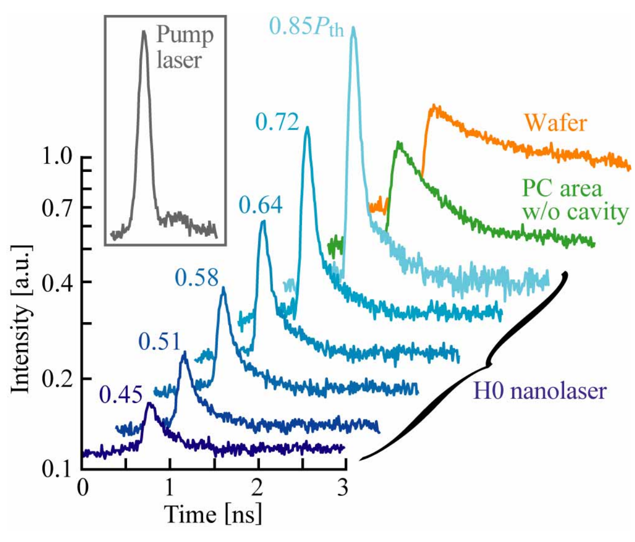

Fig. 4. SpE decay for H0 nanolaser under on-resonant condition observed at pump power of 0.45–0.85P_{th}. Results for a uniform PC area without nanocavity and an unpatterned wafer at 0.85P_{th} are also shown.

#82246 - $15.00 USD Received 19 Apr 2007; revised 28 May 2007; accepted 28 May 2007; published 4 Jun 2007

10 ps order. Figure 4 shows the on-resonant emission decay for the H0 nanolaser below the lasing threshold in comparison to an unpatterned wafer and uniform PC area without a nanocavity. The typical value of τ for the wafer is 2–3 ns, shortening to <1 ns in the uniform PC area due to surface recombination at the etched sidewall of airholes. The decay lifetime of the H0 nanolaser is even shorter, <0.4 ns, influenced not only by the Purcell effect, but also by various carrier losses, as discussed below. Figure 5 summarizes the typical characteristics of the mode intensity and lifetime with respect to normalized pump power. The H0 nanolaser exhibits a rapid increase in mode intensity near the threshold and lower SpE intensity below the threshold, whereas the H1 nanolaser displays a gradual increase in mode intensity and higher SpE intensity below the threshold. Both nanolasers exhibit much shorter decay lifetimes than either the unpatterned wafer or the PC area at any pump level. In correspondence to the intensity characteristics, the lifetime of the H0 nanolaser decreases rapidly near the threshold, while the lifetime of the H1 laser decreases gradually. The dissimilarity of these characteristics was observed in all samples of these nanolasers. Notably, SpE enhancement and near-thresholdless operation are more observable for the H1 nanolaser than the H0 device, suggesting that high *Q* is not necessarily important for achieving thresholdless operation.

4. Theoretical fitting of Purcell factor

The theoretical characteristics are estimated through a rate equation analysis of the carrier density $N(x,y,z;t)$ and photon density of the laser mode $S(t)$ with respect to positions x, y, z and time t, as given by [30]

$$\frac{dN}{dt} = \frac{P_{\mathrm{pump}}}{\hbar\omega_{\mathrm{pump}}} - GSn^2|E|^2V_{\mathrm{m}} - [FCn^2|E|^2V_{\mathrm{m}} + (1-C)]BN^2 + C_{\mathrm{A}}N^3 + D\nabla^2 N \tag{1}$$

$$\frac{dS}{dt} = \int_{\mathrm{QW}} GSn^2|E|^2 dxdydz + \int_{\mathrm{QW}} FCBN^2n^2|E|^2 dxdydz - \frac{S}{\tau_{\mathrm{ph}}} \tag{2}$$

$$eN\upsilon_{\mathrm{s}} = -eD\nabla N \ \text{(at semiconductor/air boundaries)} \tag{3}$$

where P_{pump} is the pump power density, $\hbar\omega_{\mathrm{pump}}$ is the pump energy, $G(N)$ is the gain coefficient, C is the spontaneous emission coupling factor into the laser mode when the Purcell effect is not counted, B is the radiative recombination coefficient, C_{A} is the Auger recombination coefficient, D is the carrier diffusion constant, τ_{ph} is the photon lifetime determined by the passive cavity Q and the free carrier absorption loss, and υ_{s} is the surface recombination velocity. E is the electric field distribution of the laser mode, which is normalized such that $\iiint n^2|E|^2 \mathrm{d}x\mathrm{d}y\mathrm{d}z = [n^2|E|^2]_{\max}V_{\mathrm{m}} = 1$. Further details of these equations were referred to Ref. 30, except for the third term on the right side of Eq. (1). This term introduced in the present paper expresses the controlled SpE; the SpE term for the laser mode is weighted by $Fn^2|E|^2V_{\mathrm{m}}$. When $FC >> 1$, the $(1-C)$ term in parenthesis is negligible for the laser mode, and the equations become dependent only on FC. The theoretical results shown in Fig. 5 are calculated with typical parameters for the wafer [31], structural parameters of fabricated devices, cavity mode distributions with a vertical optical confinement factor into the QW of 9.2%, the experimentally evaluated Q for each laser, and the short pulse pumping condition used in the time-resolved measurement. Fitting the theoretical characteristics to the experimental plots suggests FC values of 10 and 7 for the H0 and H1 nanolasers, respectively. For the dipole mode of the H1 nanolaser, C is calculated to be 0.4 [32]. A similar value is expected for the monopole mode of the H0 nanolaser. The evaluated values of FC can be well explained by a C value of 0.4–0.5 and the theoretical F values of 25 and 13. If the $(1-C)$ term is not neglected, the SpE coupling factor enhanced by the Purcell effect can be expressed as $C' = FCn^2|E|^2V_{\mathrm{m}}/(FCn^2|E|^2V_{\mathrm{m}}+1-C)$ for a local dipole and averaged as $C' = FC/(FC+1-C)$ for dipoles distributed over the modal area in the QW. For the experimental results, averaged C'

#82246 - $15.00 USD Received 19 Apr 2007; revised 28 May 2007; accepted 28 May 2007; published 4 Jun 2007

of 0.94 and 0.92 are estimated for the H0 and H1 nanolasers, respectively. However, if the two dipole modes in the H1 nanolaser have the same F, averaged C' would be half of this value.

As can be seen in Fig. 5, despite such a large value of C', the SpE intensity below the threshold is more than two orders of magnitude lower than the ideal thresholdless level. One reason for this is the short pulse pumping in the time-resolved measurement, which leads a lower carrier density [33], longer SpE lifetime and higher carrier losses. Therefore, the intensity becomes much higher in the CW experiment, as shown in Figs. 2(d) and 3 (d). But still the intensity is 1 – 2 orders lower than the thresholdless level. This is due to various carrier losses, as explained in the next section.

5. Discussion

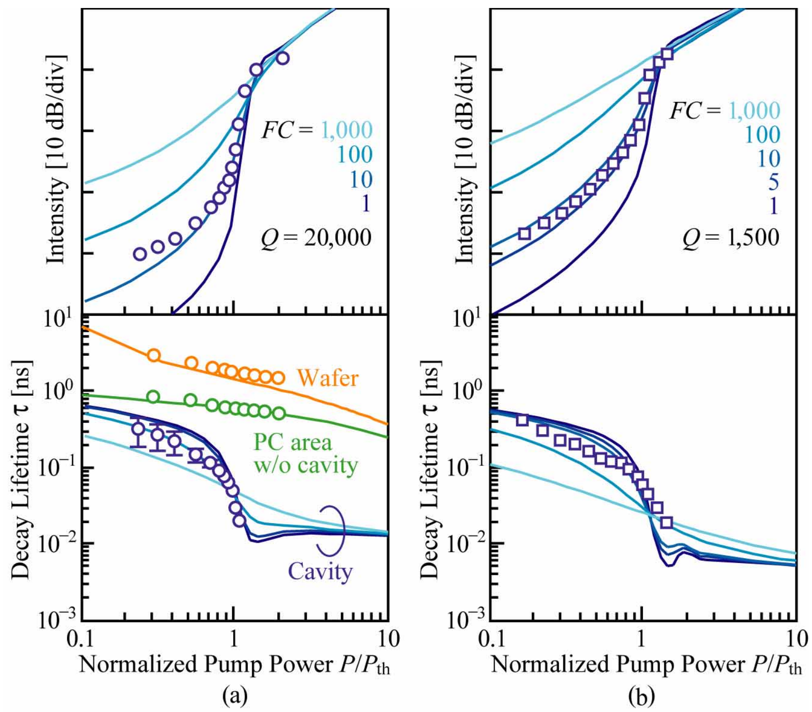

Fig. 5. Logarithmic plots of experimental and theoretical results for modal intensity (upper) and decay lifetime (lower) characteristics for pulsed measurements. (a) H0 nanolaser with Q = 20,000. Results for unpatterned wafer and PC area without cavity are also shown. (b) H1 nanolaser with Q = 1,500.

5.1. Origin of the carrier losses

In this section, carrier losses in the nanolaser and their dependence on the cavity Q are explained by the rate equation analysis. Figure 6(a) shows the laser characteristics calculated for the H0 nanolaser under CW condition. Parameters used for (A) – (D) are summarized in Table I. (A) shows the result for typical parameters of $\upsilon_s = 2 \times 10^4$ cm/s, $D = 2$ cm^2/s, and FC = 10 (F = 25, C = 0.4). The SpE intensity is attenuated two orders lower than the thresholdless level by surface recombination, carrier diffusion, and nonlaser mode emission. When the surface recombination and carrier diffusion are neglected by assuming υ_s = 0 cm/s and D = 0 cm^2/s, the SpE intensity becomes 30 times higher, as shown in (B) and (C). The remaining

#82246 - $15.00 USD   Received 19 Apr 2007; revised 28 May 2007; accepted 28 May 2007; published 4 Jun 2007

carrier loss is the nonlaser modes, which originates from the assumption C = 0.4. (When the surface recombination and carrier diffusion are neglected, (1–C) term in Eq. (1) cannot be ignored.) Actually, (D) calculated for C = 1 well traces the ideal thresholdless line. But particularly large attenuation of the SpE in (C) is caused by a photon recycling process. Figure 6(b) shows the schematic showing the carrier and photon behaviors in the cavity. In a high-Q nanocavity, emitted photons coupled to the laser mode are strongly reabsorbed below the transparent condition due to the long photon lifetime. (It is different from the so-called strong coupling regime of electron and photon, because the electronic coherent state is hardly maintained within the photon lifetime in the QW active region at RT.) The recycled carriers are partly redistributed to nonlaser mode emission, which quickly escapes from the cavity, or wasted by nonradiative recombinations. This recycling process severely accelerates carrier losses and reduces the SpE intensity.

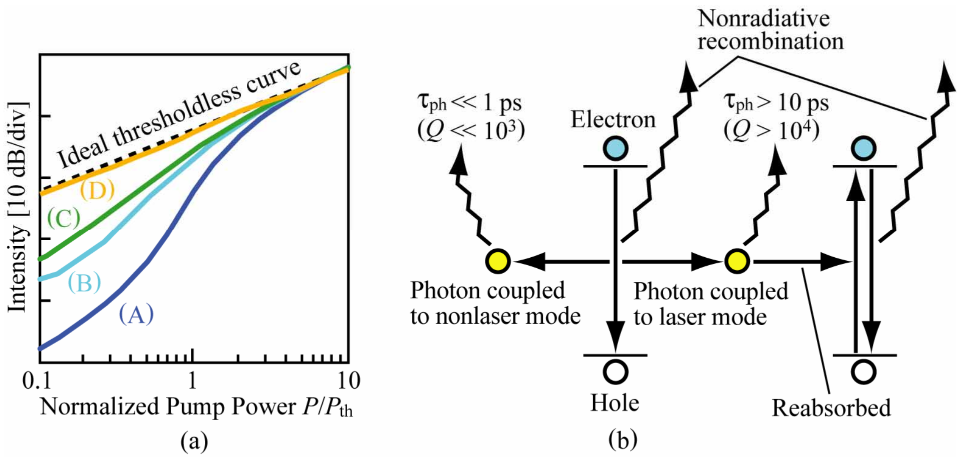

Fig. 6. SpE intensity dependence on carrier losses. (a) Calculated modal intensity characteristics for different loss parameters whose details are shown in Table I. (b) Simplified schematic of carrier and photon behaviors in the cavity.

Tabel I. Calculation parameters.

λ_{pump} = 0.98 μm	$B = 1 \times 10^{-10}$ cm^3/s	V_m = 0.019 μm^3
G = 1500 cm^{-1}	$N_{trans} = 1.5 \times 10^{18}$ cm^{-3}	Q = 20,000
n = 3.4	$C_A = 2.5 \times 10^{-29}$ cm^6/s	

(A)	$\upsilon_s = 2 \times 10^4$ cm/s	D = 2 cm^2/s	F = 25	C = 0.4
(B)	0	2	25	0.4
(C)	0	0	25	0.4
(D)	0	0	10	1.0

5.2. Discussion for effective spontaneous emission enhancement

The SpE intensity can be improved in several ways. The first one is the suppression of the surface recombination at sidewall of airholes. The surface passivation technique gives some degree of improvement [34]. The second one is the enhancement of the Purcell factor F. For a large F, the SpE rate for the laser mode becomes higher than the nonradiative recombination rate, and the spatial hole burning of carriers formed by the intensified mode suppresses the

#82246 - $15.00 USD Received 19 Apr 2007; revised 28 May 2007; accepted 28 May 2007; published 4 Jun 2007

carrier diffusion to outside of the cavity. In addition, the coupling of SpE to nonlaser modes is relatively suppressed. As a result, the SpE intensity is enhanced almost in proportional to *F*, as shown in Fig. 7(a). However, *F* in this experiment cannot be enhanced by the cavity *Q* but constrained by the homogeneous broadening. Therefore, a significant enhancement is not expected without employing another material with a narrower homogeneous broadening. The third one is the optimization of the cavity *Q*. Figure 7(b) shows the intensity characteristics calculated against different *Q*s. As mentioned above, a high *Q* accelerates carrier losses through the photon recycling process. The SpE intensity is clearly enhanced for lower *Q*, even though the threshold also increases.

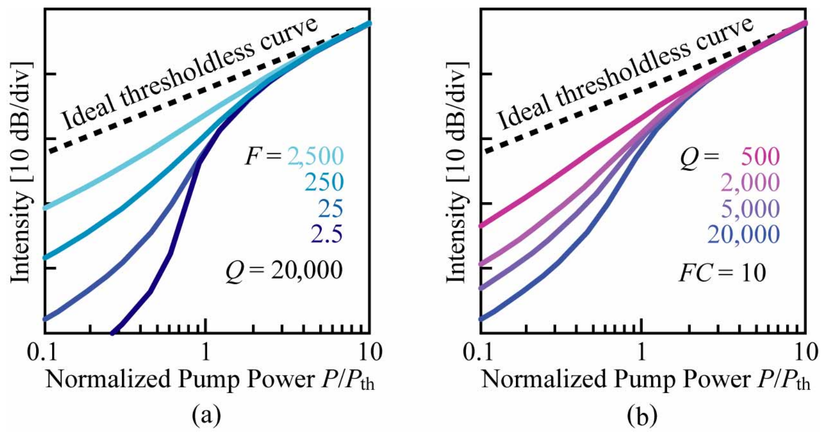

Fig. 7. Calculated modal intensity characteristics, where *F* and cavity *Q* are taken as a parameter for (a) and (b), respectively. Other parameters are the same as for (A) in Fig. 5.

6. Conclusion

In this paper, an ultimately small PC nanolaser was fabricated using a HI-based fine etching process of GaInAsP wafers and the RT CW operation was demonstrated for the first time. The fabricated device has a high *Q* factor of 20,000 and an effective lasing threshold of just 1.2 μW. The enhanced SpE rate due to the Purcell effect was evaluated carefully through time-domain measurements. The product of the Purcell factor and the SpE coupling factor, *FC*, was estimated to be 10 for this nanolaser. The observed characteristics were well explained by a detailed rate equation analysis, with the results indicating that carrier losses and photon recycling process in a device with unnecessarily high *Q* degrade the SpE intensity below the lasing threshold. Actually, near-thresholdless operation was observed in a device with a low *Q* of 1500. Thus, a high *Q* is desirable for low threshold laser operation, while a moderately low *Q* is effective when high efficiency modal emission below threshold is particularly expected in such applications as a single photon emitter.

Acknowledgment

This work was supported by the Core Research for Evolutional Science and Technology (CREST) Project of the Japan Science and Technology (JST) Agency, by a Grant-in-Aid, the Focused Research and Development Project for the Realization of the World's Most Advanced IT Nation, and the 21st Century Center of Excellence (COE) Program of the Ministry of Education, Culture, Sports, Science and Technology of Japan, and by a Grant-In-Aid and a Research Fellowship from the Japan Society for the Promotion of Science (JSPS).